"CREATOR Case": PMSM and IM Electric Machine Data for Validation and Benchmarking of Simulation and Modeling Approaches

Abstract

Purpose – This paper describes the complete sets of data of two different machines, a PMSM and an IM, that are made available to the public for modeling and simulation validation and benchmarking.

Design/methodology/approach – For both machines, not only the complete sets of design parameters, i.e., motor geometry, electrical parameters, material properties, and winding schemes as well as the measured low-frequency equivalent circuit parameters are provided, but also comprehensive measurement results on six different drive cycles to allow for transient investigations.

Findings – The data packages provide all the required information in terms of design parameters and measurement results that facilitate modeling and simulation validation and benchmarking results for verification of different modeling approaches.

Research limitations/implications – The paper serves as the key reference user manual for the extensive and comprehensive sets of data made available. It is therefore recommended to follow up on the reading of the paper by a study of the data packages themselves.

Originality/value – To the authors' best knowledge, this is the first time that the complete sets of machine data of two different machines are published, allowing for benchmarking of modeling and simulation projects, and reproducibility and reusability following the FAIR data principle of analyses based on these data.

Keywords – Electric machines, design data, measurement results, modeling, reusability, simulation, verification, validation.

Paper type: Research paper.

1 Motivation

The tedious design process of electric machines, that involves different disciplines, e.g., electrical, mechanical, magnetic, and thermal aspects, and also increasingly dynamic analyses, calls for example cases for benchmarking of modeling and simulation approaches. Today, the literature only presents selected machine design-related data and shows the laboratory results of chosen parameters or performance criteria. As verification and validation of models has become increasingly important, so has the need for the availability of data to allow for verification and validation of models, as well as reproducibility and reusability of results (Oberkampf and Roy, 2010). To this aim, and to the authors' best knowledge for the first time, we publish the complete sets of machine data for two different machines for such multifaceted analysis. These packages of data provide all the required information in terms of design parameters and measurement results to facilitate their use as validation and benchmarking tool for different modeling approaches, beyond the specific quantitative results as obtained from singular analyses (Bergfried et al., 2023).

2 Introduction

Electric machines, as key players in energy conversion, have been known for more than a century. The recent technological advancements in electric drives and power electronic systems, together with new materials and manufacturing techniques and increasingly transient performance requirements, provide plenty of opportunities for future innovations, but also increase the demands on the modeling and simulation tools, e.g., Ahn et al. (2023); Hwang et al. (2021). Current electric machine design procedures usually start with an expert's choice for a particular machine type and topology or already-developed design choices, e.g., Barcaro and Bianchi (2013); Krause et al. (2013); Mese et al. (2016). Optimization is then typically based on selected parameters and steady-state operating points, e.g., Rimpas et al. (2023); Gobbi et al. (2024); Li et al. (2017). However, exploiting the

full potential of electric machines in the future requires more powerful approaches to account for the different design possibilities, parameters, and criteria. We provide all data relevant for the comprehensive modeling of two machines, as well as measurement results for both selected steady-state operating points and three different drive cycles, to allow for code validation or benchmarking, e.g., as a baseline for innovative shape or topology optimization techniques. As a matter of fact, well-prepared experimental data is incredibly valuable for the validation of simulation models and available data can underpin the reliability and reproducibility of the results for the community (Weinper and Tomczak, 2021). We thereby also contribute to increasing availability of results in the field of electric machines that follow the FAIR (Findability, Accessibility, Interoperability, and Reusability) principles, which enables transparency and reproducibility of research knowledge, an acronym introduced almost a decade ago by a consortium of scientists and organizations (Wilkinson et al., 2016). In contrast to the reporting of selected results without context, e.g., on data science competition platforms Fedesoriano (2021); Shimizu (2023); Ferretti (2022) and to the problems formulated by the TEAM (Testing Electromagnetic Analysis Methods) initiative (*TEAM Problems – International Compumag Society*, 2018) or the Galileo Ferraris Contest (*Gallileo Ferraris Contest*, 2024), we are not posing a specific challenge.

3 The Example Case Machines

The Collaborative Research Centre "Computational Electric Machine Laboratory - CREATOR" (CRC – TRR361 /F90) (Österreichischer Wissenschaftsfonds FWF, 2022; Deutsche Forschungsgemeinschaft DFG, 2022) aims at enhancing electric machine performance and computational efficiency by bringing together advances in many different disciplines. As part of this project, essential design and measurement data of electric machines are obtained and shall be made available to many other researchers within the community. The work that generates the data on these example motors itself assesses the performances of different modeling approaches to analyze dynamic drive cycle operation, including the crucial experimental validation.

The two motors are available and analyzed in the Electric Drives and Power Electronic Systems Institute (EALS) laboratory at TU GRAZ, an induction motor (IM) and a permanent magnet synchronous motor (PMSM). While the machines were originally not optimized for traction applications, both are machines designed for research purposes, with all relevant data available and some characteristics that make them notably interesting for research – and also benchmarking – purposes.

The machine design and measurement data packages are made available through two central repositories, Heidarikani (2024) and Dhakal (2024), one for each of the two machines. They are discussed and analyzed in Sections 5 and 6, respectively, for each of the two machines. Prior to this, the next Section outlines the organization of these two main parts of the paper.

4 Data and Data Presentation Organization

Subsections 5.1 and 6.1 detail the repositories of the design data parameters for both the IM and the PMSM, respectively. They provide a structured framework for analysis and comparison. Within these subsections, each part is dedicated to a specific aspect of the motors' designs, as follows: Sub-subsections 5.1.1 and 6.1.1 detail the motor geometries, 5.1.2 and 6.1.2 the material properties, 5.1.3 and 6.1.3 the electrical parameters and 5.1.4, and 6.1.4 the winding schemes of the IM and the PMSM, respectively.

In Subsections 5.2 and 6.2, the repository also provides comprehensive measurement results concerning both the IM's and the PMSM's conventional operating characteristics such as no-load tests for both motors (6.2.1 and 5.2.1, respectively) and the locked rotor test specifically for the IM 5.2.1, as well as the derivation of equivalent circuit parameters from measurement data (5.2.2 and 6.2.2, respectively).

In addition to these steady-state characteristics, the repository provides extensive measurement results of drive cycles, i.e., predefined sequences of torque-speed pairs over time for the analysis of dynamic drive performance. Three standard reference drive cycles are selected to evaluate the performance of electric machines in traction electrification: the WLTP (worldwide harmonized light vehicles test procedure), the Braunschweig city drive cycle (urban), and the Artemis 130 km/h drive cycle (inter-city) (DieselNet, 2011), see Figure 1. The WLTP offers a balanced representation of urban, suburban, and highway driving scenarios. The urban drive cycle emphasizes low-speed, high-torque conditions, crucial for assessing city driving performance characterized by frequent stops and starts. The inter-city drive cycle examines moderate speeds and less frequent stops, reflecting typical conditions encountered during inter-city commutes.

To derive the required torque and speed for each drive cycle, two reference vehicles are considered: the BMW i3 (medium range) and the Smart EQ (small range), employing their specifications in quasi-static longitudinal vehicle models (Guzzella and Amstutz, 2005). Inputting the drive cycle into the longitudinal vehicle model of
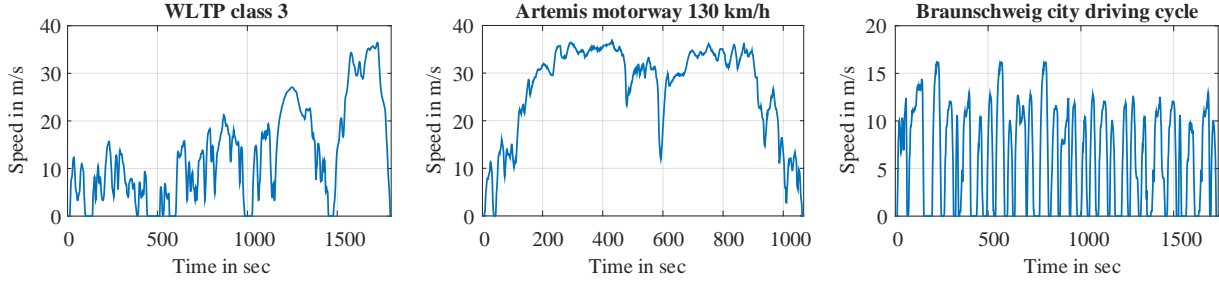
Fig. 1: Standard reference drive cycles; available e.g. on DieselNet (2011).

each EV determines the required torque and speed on the wheels of the vehicle. The necessary torque and speed of the vehicle motor can then be determined by utilizing the gear transmission. However, since the rating of the vehicle motor may differ from that of the motors in the laboratory, a down-scaling method is employed to ensure that the input data falls within the range of the IM and the PMSM in the laboratory. Detailed information about the down-scaling method, the longitudinal vehicle model, and vehicle data is presented in Dhakal et al. (2023).

Schematic overviews of the test benches and the control architectures for both motors are provided in Appendices A and B, respectively.

Sub-subsections 5.2.3 and 6.2.3 discuss the input drive cycle torque and speed data for the six cases (3 cycles, 2 vehicles) per motor as well as the corresponding measurement results for both machines, including the output and input power and the measured losses of the IM and of the PMSM, respectively.

5 Induction Motor

The three-phase squirrel cage IM is completely enclosed and water-cooled to maintain optimal performance under varying conditions. With a total of 92 temperature sensors strategically integrated, this motor enables comprehensive temperature analysis, as it was originally manufactured for analysis of temperature distribution under post-fault operation (Eickhoff et al., 2021).

Figure 2 shows the picture of the motor and its completed stator winding during the manufacturing process. All IM related data and experimental results are made available online through the central repository Heidarikani (2024). Table 1 summarizes the general parameters of the IM.

Tab. 1: General design parameters of the IM.

Parameter	Value	Unit
Rated speed	1430	rpm
Maximum speed	2900	rpm
Rated torque	24.7	Nm
Maximum torque	31	Nm
Rotor moment of inertia	0.039	$\mathrm{kg\,m^2}$
Cooling system	Totally enclosed water cooled	–

5.1 Design Parameters

5.1.1 Motor Geometry

Figure 3 shows a 2D CAD drawing of the motor, with complete dimensions, detailing the motor housing, rotor, stator, and windings. Additional geometric data essential for modeling the IM, such as details on the end ring, end winding, and housing, are provided in Appendix A. The online repository also contains pre-built geometry model files for ease of use.

5.1.2 Material Properties

Table 2 shows the materials utilized in the different components of the IM. For each material, the corresponding online data repository link is cited.
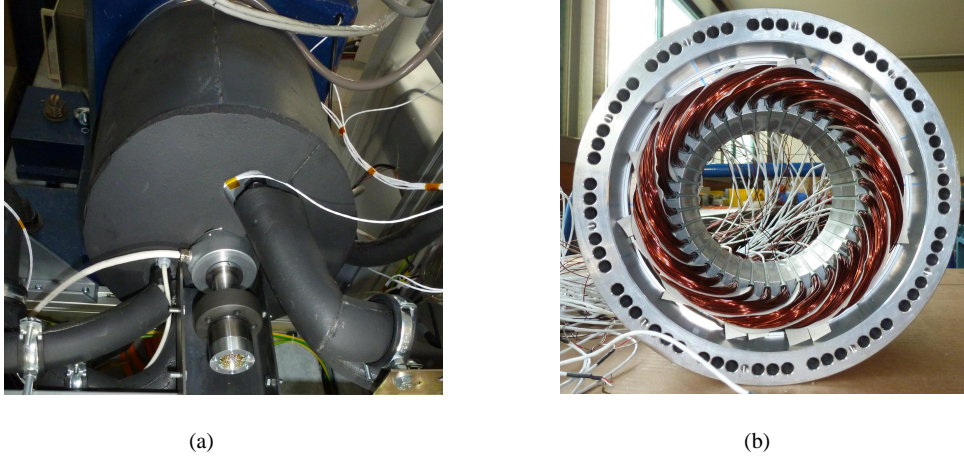
Fig. 2: The example-case IM prototype: (a) non-drive side with rotary encoder and insulating layer over cooling jacket, (b) completed stator winding before rotor installation.
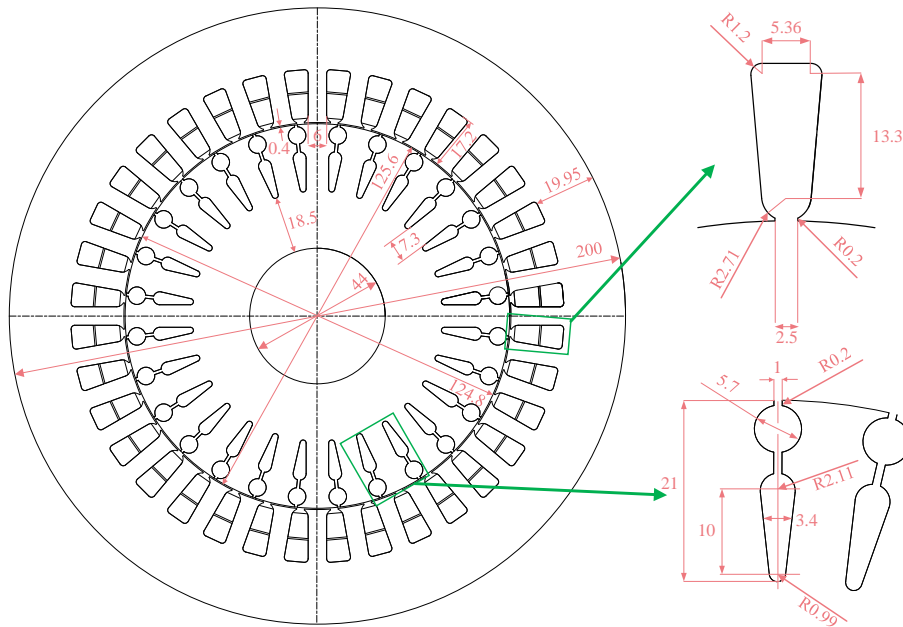
Fig. 3: 2D CAD diagram of the IM with dimensions.

Tab. 2: Material parameters of the IM.

Part	Material
Stator and rotor iron	Electrical steel sheet M800 − 50A
Shaft	Steel 1 7225/42CrMo4
Rotor cage and cooling jacket	Aluminium 6082/3.2315
Stator winding	Copper
Slot liners and winding overhang insulation	Trivoltherm NRN
Stator winding insulation	Elan-tron MC 4260/W 4260

5.1.3 Electrical Parameters

Table 3 provides the electrical parameters of the IM.

5.1.4 Winding Scheme

An overview of the winding scheme is presented here. To this aim, Table 4 details the parameters of the winding of the IM, Figure 4 visually illustrates the coil designations for all phases, showing the winding arrangement

Tab. 3: Electrical properties of the IM.

Parameter	Value	Unit
Maximum power	4.6	kW
Nominal power	3.7	kW
Nominal voltage	400	$V\,rms, L-L$
Maximum dc-link voltage	640	V
Nominal current	6.9	A rms
Maximum current	15	A rms
Supply connection	Y	–
Nominal frequency	50	Hz
Maximum frequency	100	Hz

within the motor.

Tab. 4: Winding properties of the IM.

Parameter	Value	Unit
Winding type	Dual layer distributed winding	–
No. of phases	3	–
Slot per pole and phase	3	–
No. of turns per layer	18	–
No. of stator layer	2	–
Wire diameter	2×0.75	mm
Coil pitching	7/9	–

5.2 Measurement Results

5.2.1 No-Load and Locked Rotor Tests

The no-load test evaluates the IM performance without mechanical load. From this, selected parameters such as core loss, magnetization current, and magnetization inductance can be identified. Conversely, in the locked-rotor test, the motor is mechanically prevented from rotating, and voltage, respectively currents are applied to determine impedance parameters such as rotor resistance and leakage inductances. For more explanations on these tests, see, e.g., Hendershot and Miller (2010); Pyrhonen et al. (2009).

Both tests were carried out for different supply frequencies and amplitudes. Figure 5 shows the iron and the sum of friction and windage losses as derived from the measurements, for different supply frequencies and flux linkages. To separate the losses, the measurement results were separated into their frequency-dependent and frequency-independent parts.

5.2.2 Equivalent Circuit Parameters

The equivalent circuit parameters of the IM, as derived from the measurements, are shown in Table 5. The stator resistance (R_s) was measured through a direct current test, the rotor resistance (R_r) determined from the locked-rotor test. The stator magnetization inductance (L_m) was derived from a no-load test , and the combined leakage inductance ($L_{\sigma\mathrm{s}} + L_{\sigma\mathrm{r}}$) was calculated from the locked-rotor test. Due to motor symmetry, the two leakage inductances $L_{\sigma\mathrm{s}}$ and $L_{\sigma\mathrm{r}}$ are assumed to be equal (Tessarolo et al., 2015).

Tab. 5: Equivalent circuit parameters of the IM.

Parameter	Value	Unit
Stator resistance R_s at 20 °C	2.329852	Ω
Rotor resistance R_r at 20 °C	1.011977	Ω
Stator leakage inductance $L_{\sigma\mathrm{s}}$	0.0114450	H
Rotor leakage inductance $L_{\sigma\mathrm{r}}$	0.010648	H
Reference magnetization inductance of stator L_m	0.226	H

Figure 6 shows the measured magnetization flux (λ_m) versus current (I_m) and the derived current-dependent inductance (L_m). Figure 7 displays the variation of the rotor resistance with frequency, as well as the relationship
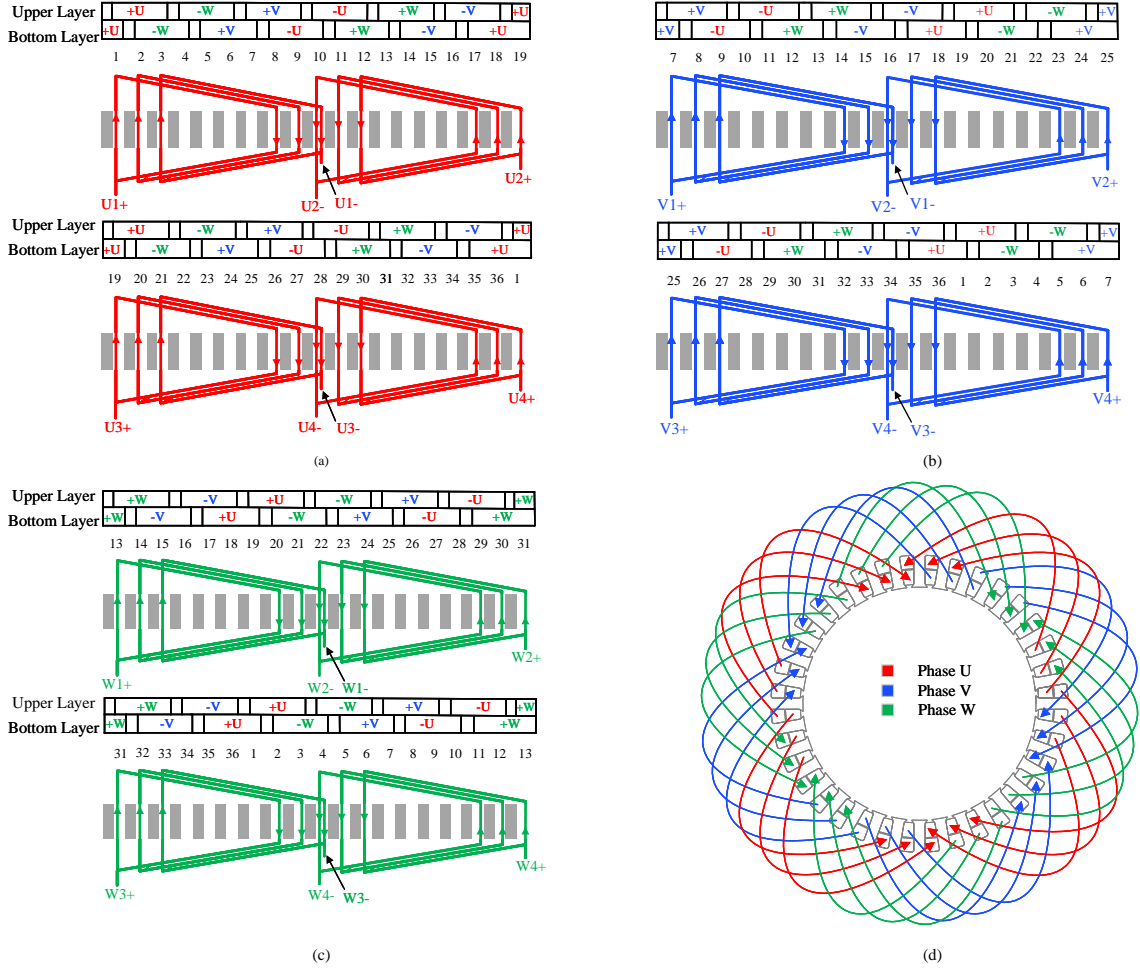
Fig. 4: Winding scheme of the IM: (a) slot view of phase U, (b) slot view of phase V, (c) slot view of phase W, (d) model view of all three phases.
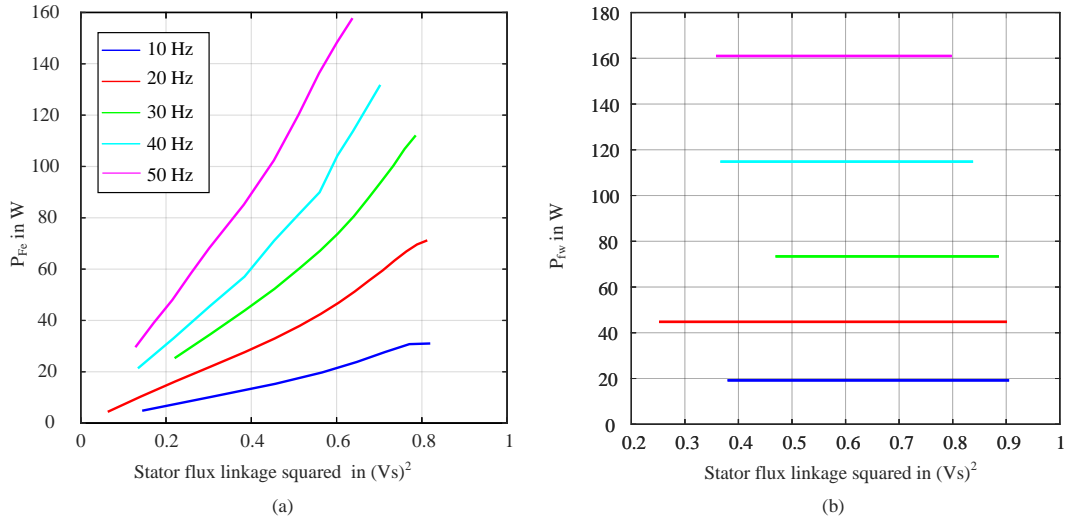
Fig. 5: Core and friction losses derived from no-load tests: (a) core loss, (b) sum of friction and windage losses.

between stator and rotor leakage inductances and frequency. The low-frequency single-phase equivalent circuit of the IM is shown in Appendix A.
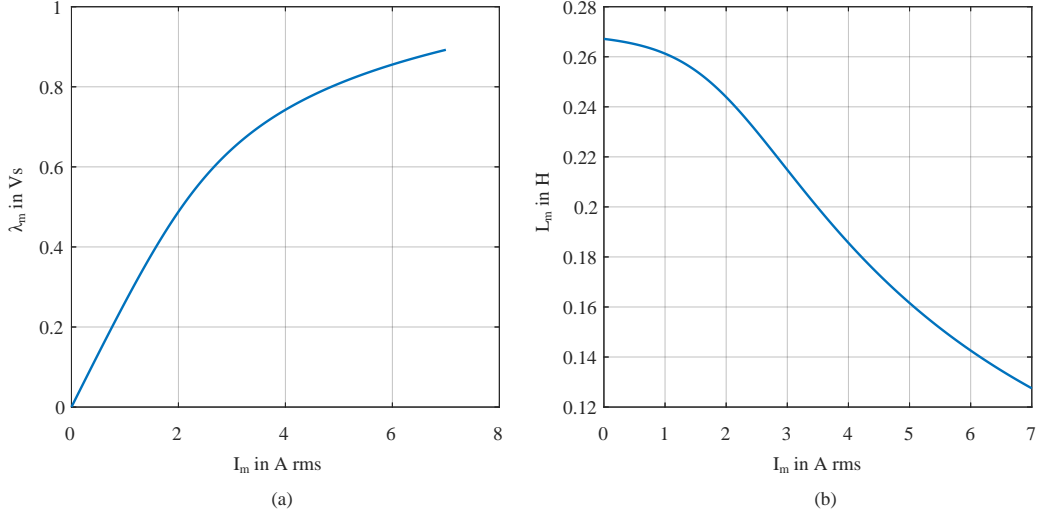
Fig. 6: Measured magnetization characteristic of the IM: (a) λ_m vs I_m, (b) L_m vs I_m.
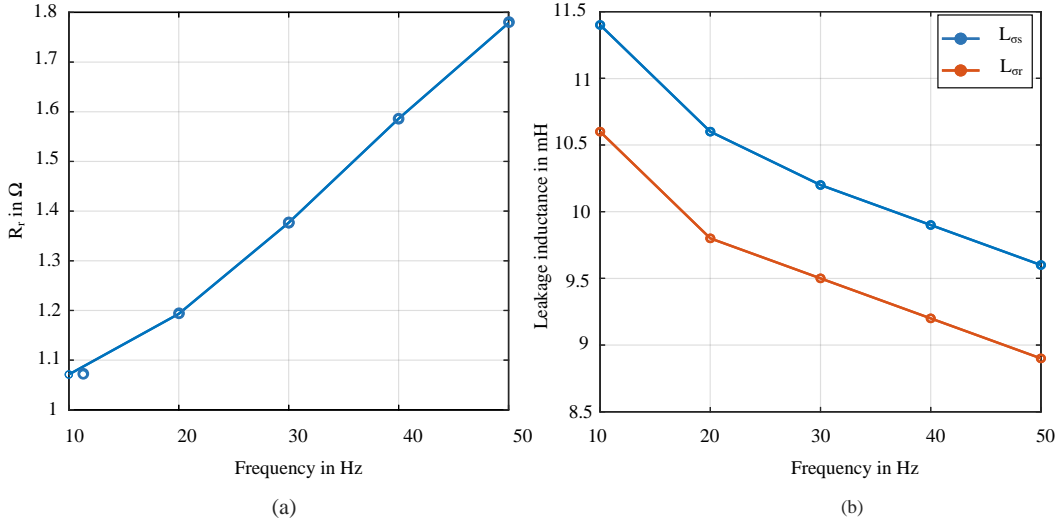
Fig. 7: Measured rotor resistance and leakage inductances as a function of frequency: (a) R_r, (b) $L_{\sigma s}$ and $L_{\sigma r}$.

5.2.3 Drive Cycles

An exemplary case of the analysis of the WLTP class 3 drive cycle for the IM, utilizing the down-scaling procedure (Dhakal et al., 2023) based on the specifications of a medium-sized vehicle (BMW i3), is presented. It covers both the input data for the measurement, i.e., the torque and the speed, as well as the measured output data of the IM throughout the entire drive cycle. The measured input and output powers, along with the total loss calculated from the measurement, as well as the input torque and speed profiles are shown in Figure 8. The online repository is not limited to the single drive cycle case depicted in this example; it holds complete measurement data for the six cases of both vehicles and three drive cycles.

6 PM Synchronous Motor

The PMSM machine presented here is a prototype inset PM machine originally designed for use in high-efficiency household cooling appliances with a maximum continuous power of 70 W and a targeted optimum performance at 7 W. With a maximum continous power and maximum efficiency occurring at different operting points, it reflects demands on many modern motors, notably used in traction applications. The prototype machine, shown in Figure 9, is naturally cooled and designed to run long hours with considerably high efficiency. All PMSM related data and experimental results are made available online through the central repository Dhakal (2024). Table 6 describes the general design parameters of the PMSM.
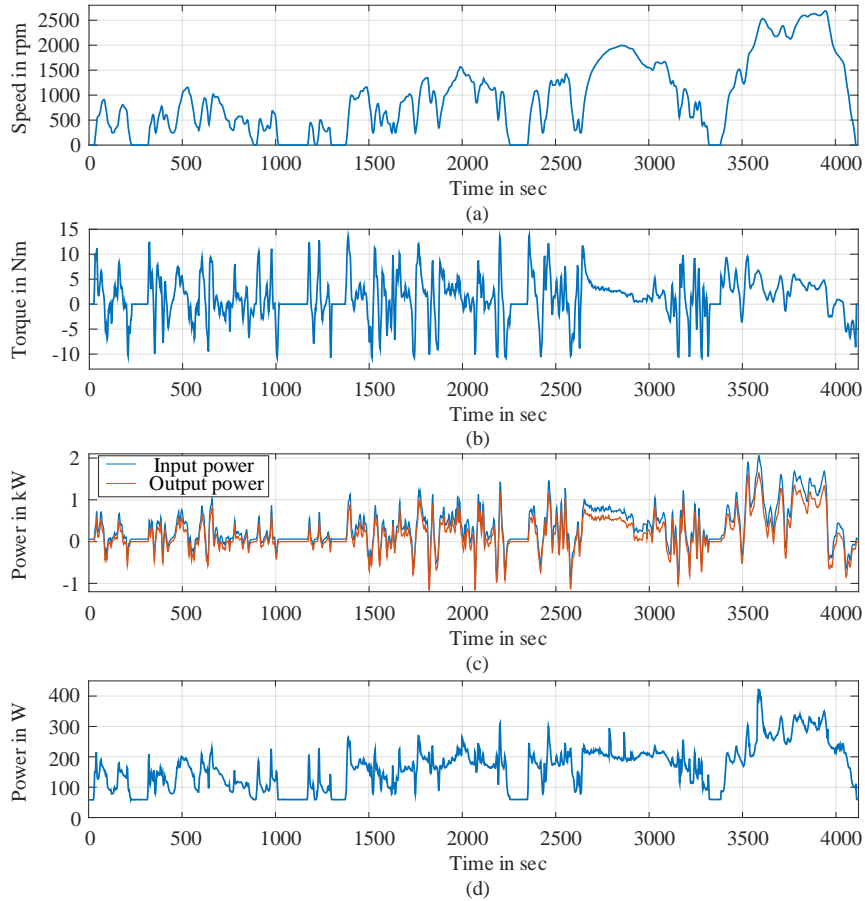
Fig. 8: Measurement results of WLTP class 3 drive cycle for the IM: (a) speed profile of the down-scaled drive cycle, (b) torque profile of the down-scaled drive cycle, (c) measured input and output powers, (d) calculated total losses.

Fig. 9: PMSM prototype.

6.1 Design Parameters

6.1.1 Motor Geometry

A 2D geometry diagram of the PMSM is illustrated in Figure 10. The stator, rotor, and magnet dimensions are highlighted. Table 12 details the motor geometry. For ease of use, pre-built geometry model files are also available in the online repository.

Tab. 6: General design parameters of the PMSM.

Parameter	Value	Unit
Rated speed	2000	rpm
Maximum speed	7050	rpm
Rated torque	0.10	Nm
Maximum torque	0.15	Nm
Rotor moment of inertia	0.00011348	$\mathrm{kg\,m^2}$
Cooling system	Naturally cooled	–
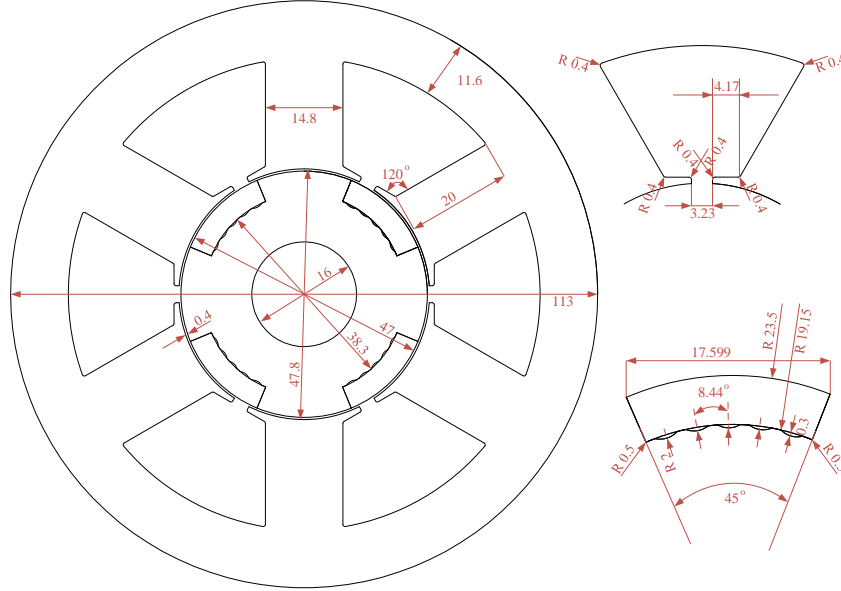
Fig. 10: 2D CAD diagram of the PMSM with dimensions.

6.1.2 Motor Material

Table 7 details the motor parts and the corresponding material used. For each material, the corresponding online repository link is cited.

Tab. 7: Material parameters of the PMSM.

Part	Material
Stator and rotor iron	Electrical steel M250 − 35A
Stator winding	Copper
Magnet	Sintered ferrite radially magnetized
Shaft	–

6.1.3 Electrical Parameters

Table 8 provides the electrical parameters of the PMSM.

6.1.4 Winding Scheme

Here, the winding scheme of the PMSM is presented. Table 9 details the winding properties, Figure 11 shows its model and the slot view.

6.2 Measurement results

6.2.1 No-Load Tests

No-load tests of the PMSM are carried out to assess the load-independent losses within the motor itself, such as iron and frictional losses, and to assess the machine parameters, such as back-EMF and cogging torque. For

Tab. 8: Electrical parameters of the PMSM.

Parameter	Value	Unit
Maximum power	70	W
Optimum power	7	W
Nominal voltage	135	V rms
Maximum dc-link voltage	326	V
Nominal current	0.21	A rms
Maximum current	0.3	A rms
Supply connection	Y	–
Nominal frequency	66.67	Hz
Maximum frequency	235	Hz

Tab. 9: Winding properties of the PMSM.

Parameter	Value	Unit
Winding type	Tooth wound/concentrated winding	–
No. of phases	3	–
Slot per pole per phase	0.5	–
No. of turns per slot	328	–
No. of winding layer	1	–
Copper wire diameter	0.64	mm
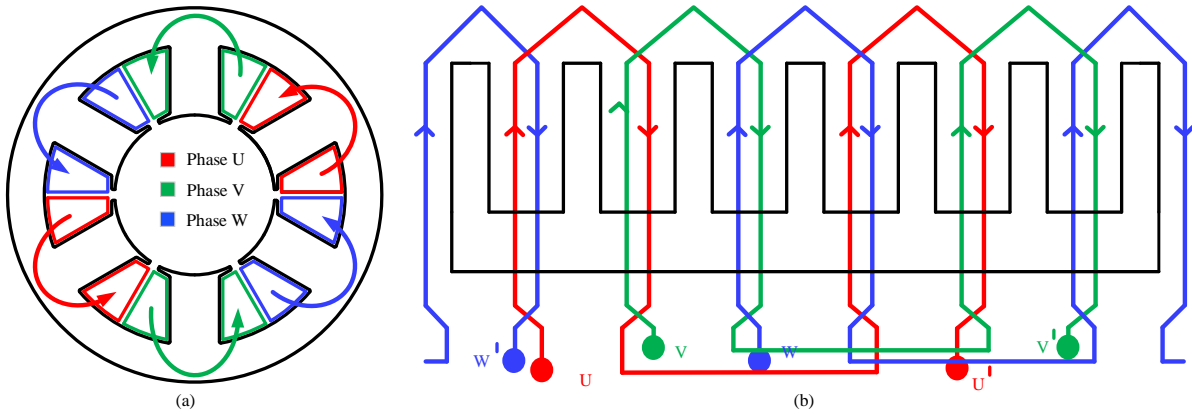
Fig. 11: Winding scheme of the PMSM: (a) model view, (b) slot view.

more explanations on such kinds of tests, see, e.g., Hendershot and Miller (2010); Pyrhonen et al. (2009). The PMSM is tested under no-load, both with the rotor mounted within the stator and without rotor (to identify the iron loss), at different rotor speeds. Figure 12 shows the no-load torque measurement results as function of speed and the calculated no-load iron losses as function of supply frequency.
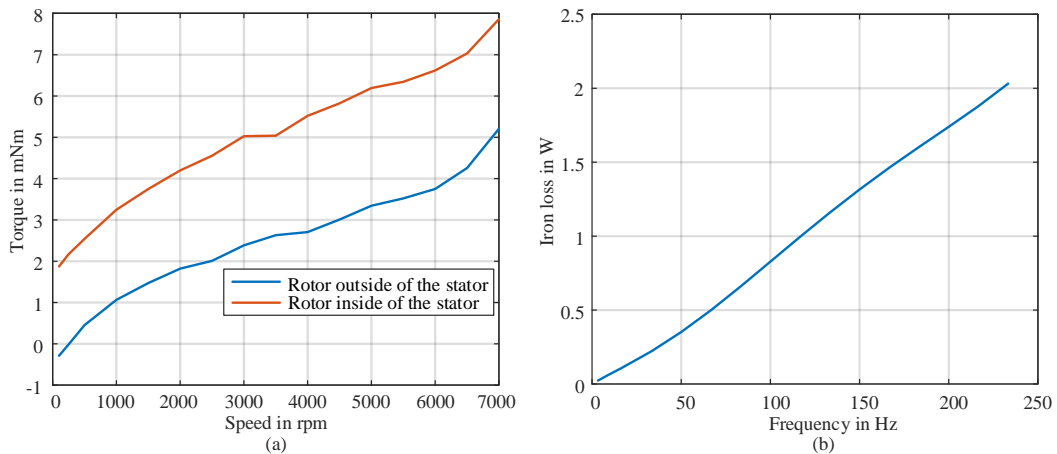
Fig. 12: No-load measurement results of the PMSM: (a) torque for rotor inside and outside of the stator, (b) calculated iron losses.
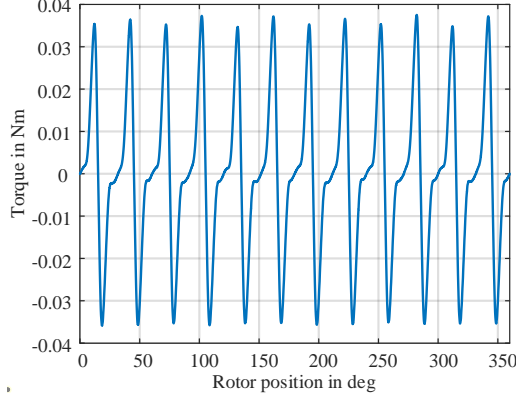
Fig. 13: Cogging torque measurement result of the PMSM.

For the measurement of the cogging torque, the rotor is rotated very slowly, at 0.25 rpm. The torque measurements are taken by a torque transducer. To measure the back-EMF, the rotor was rotated at a constant speed of 2000 rpm. The results are shown in Figures 13 and 14, respectively. A fundamental peak component of the induced back-EMF of 47.5 V per phase is identified by discrete Fourier transform.
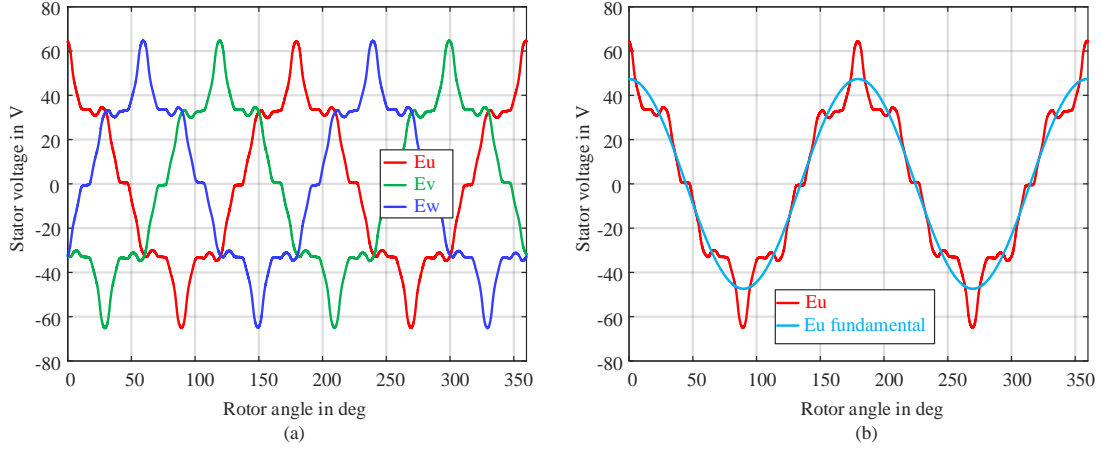
Fig. 14: Measured back emf of the PMSM: (a) voltages induced in the three phases of the stator (u, v, and w), (b) fundamental voltage component of the u phase.

6.2.2 Equivalent Circuit Parameters

Table 10 shows the low-frequency equivalent circuit parameters of the PMSM. The stator resistance is measured directly using an LCR meter (*LCR meter*, 2023). The d-axis and the q-axis inductances are obtained through finite element analysis (FEA) using the JMAG® software's (JSOL Corporation, 1983) inductance calculator tool (JSOL Corporation, 2022). An exemplary 2D JMAG model file used for this analysis is also made available in the repository.

Tab. 10: Equivalent circuit parameters of the PMSM.

Parameter	Value	Unit
Fundamental back emf at 2000 rpm, E_0	47.37	V peak
Cogging torque at 0.25 rpm	0.0357	Nm peak
Magnet flux linkage, λ_{pm}	0.1144	Wb
Stator inductance d-axis, L_{d}	0.2055	H
Stator inductance q-axis, L_{q}	0.3320	H
Stator phase resistance, R_{s}	8.9462	Ω

To calculate the current angle for maximum torque, the current angle was varied from 90°el. to 120°el., with current amplitudes of 0.15 A and 0.3 A. The motor was set to operate under motoring operating points at a

constant speed of 2000 rpm. The torque was measured as the current angle was varied and the angle that gives the maximum torque value is identified. The maximum current angles with current amplitude of 0.15 A and 0.3 A are found to be $100°_{el.}$ and $110°_{el.}$, respectively. The low frequency single phase equivalent circuit models of the PMSM are provided in Appendix B.

6.2.3 Drive Cycles

Exemplarily, the measurement results of the WLTP class 3 drive cycle with reference to the medium-sized passenger car (BMW i3), down-scaled to the PMSM as per Dhakal et al. (2023), are shown here, see Figure 15. They include the drive cycle input speed and torque, the input power, the output power, and the total losses throughout the whole drive cycle. The online repository contains the complete set of measurement data for both vehicles and all three drive cycles.
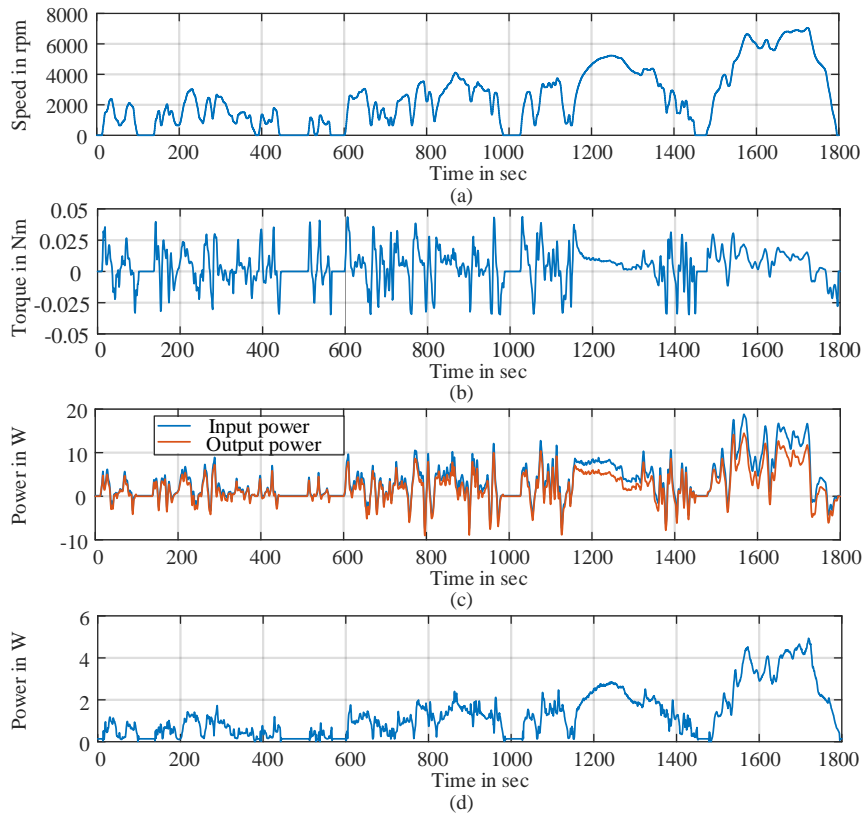
Fig. 15: Measurement results of WLTP class 3 drive cycle for the PMSM: (a) speed profile of the down-scaled drive cycle, (b) torque profile of the down-scaled drive cycle, (c) measured input and output powers, (d) calculated total losses.

7 Conclusion

This paper presents comprehensive electric machine design parameters and measurement results of two different electric machines and for a large set of six drive cycles per machine. It makes all relevant design data available for benchmarking of modeling and simulation approaches. This paper not only describes the data itself but also guides the prospective user through their organization within the repository.

Acknowledgment

Appendix A

Geometry of the IM

The detailed geometric parameters of the IM are listed in Table 11.

Tab. 11: Main geometry parameters of the IM.

Parameter	Value	Unit
Thickness of housing	0.015	m
Length of housing	0.23	m
Stator iron inner diameter	0.1256	m
Stator iron outer diameter	0.2	m
Length of stator iron	0.1	m
Length of stator teeth	0.0172	m
Width of stator teeth (equivalent)	0.0062	m
Stator slot opening	0.0025	m
Average wire radius	0.0031	m
Stator end winding length	0.03	m
Stator end winding inner diameter	0.135	m
Stator end winding outer diameter	0.18	m
Stator slot fill factor	30	%
No. of stator slots	36	–
Rotor core inner diameter	0.044	m
Rotor core outer diameter	0.1248	m
Rotor end ring length (axial)	0.014	m
Rotor end ring inner diameter	0.081	m
Rotor end ring outer diameter	0.1242	m
Rotor slot average width	0.0034	m
Rotor slot average height	0.021	m
No. of rotor cage bars	28	–
Motor air gap	0.0004	m
No. of poles	4	–

Equivalent Circuit Model of the IM

As is common for simplicity, the IEEE single-phase equivalent circuit model (ECM) of the IM is presented without considering core losses, as shown in Figure 16 (Kojooyan-Jafari et al., 2015). The diagram illustrates the per-phase equivalent circuit of the IM, where the rotor-side impedances are converted to the stator side. In the circuit, R_s and R_r represent the stator and rotor resistances (referred to the stator side), while $L_{\sigma s}$ and $L_{\sigma r'}$ denote the stator and rotor leakage inductances. The magnetization inductance is represented by L_m. Additionally, the stator voltage V_s, rotor voltage V_r, stator current I_s, and rotor current I_r are depicted. The values of the equivalent circuit parameters for the IM can be found in Table 5.
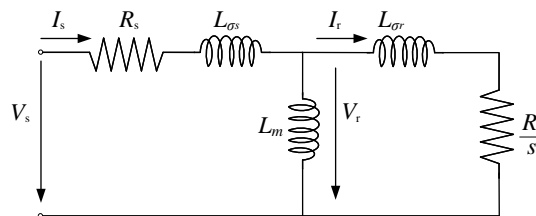
Fig. 16: Single phase ECM of an IM.

Laboratory Test Setup and Control Architecture of the IM

Rotor field-oriented control (RFOC) is utilized to control the speed of the IM, here the device under test (DUT). Additionally, the torque control is applied to the PMSM, which functions as the load machine. The control architecture illustrated in Figure 17 outlines the comprehensive control scheme utilized in the laboratory's IM

test bench. Both inverters use space vector pulse width modulation (SVPWM), at a constant switching frequency of 5 kHz.
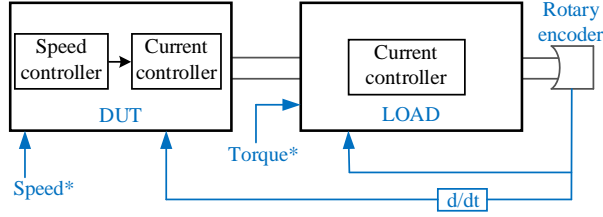
Fig. 17: Control scheme for the drive cycle of the IM on the laboratory test bench, where * denotes the commanded values.

Appendix B

Geometry of the PMSM

Table 12 lists the detailed geometry parameters of the PMSM.

Tab. 12: Main geometry parameters of the PMSM.

Parameter	Value	Unit
Stator outer diameter	113	mm
Stator inner diameter	47.8	mm
Width of back iron	11.6	mm
Slot height (equivalent)	19.6	mm
Slot width (equivalent)	21.6	mm
Width of slot opening	3.23	mm
Height of slot opening	0.98	mm
Stator slot fill factor	0.5	–
Tooth height (equivalent)	20	mm
Tooth width (equivalent)	14.8	mm
Rotor outer diameter	47	mm
Air-gap length	0.4	mm
Magnet length (radial direction)	4.35	mm
Magnet height	17.6	mm
Magnet span	45	° mechanical
Shaft diameter	16	mm
Motor length	30.1	mm
No. of poles	4	–
No. of stator slots	6	–
Stator end winding length	11.4	mm
Thickness of stator and rotor lamination	0.35	mm

Equivalent Circuit Model of the PMSM

In the majority of analyzed PMSM cases, single-phase ECMs are presented, disregarding the core loss component (Ba et al., 2022). Simplified ECMs of a PMSM are demonstrated in Figure 18. Figure 18(a) presents the single phase ECM of a PMSM. As presented in the diagram, R_s is the per-phase resistance of the stator winding and L_s is the synchronous inductance, which is an equivalent inductance of self and mutual per-phase inductances. The flux linkage of permanent magnets is denoted by λ_pm. The back electromotive force, E_0 is proportional to the electrical rotational frequency ω_e. The single phase current and voltage are denoted by I_p and V_p, respectively. Figure 18(b, c), represent the corresponding d and q-axis ECMs, respectively. As denoted in the diagram, V_d and V_q are the d nad q-axis terminal voltages, and I_d and I_q are the d and q-axis armature currents. The d and q-axis inductances are denoted by L_d and L_q, respectively. The corresponding equivalent circuit parameter values of the PMSM can be refereed from Table 10.
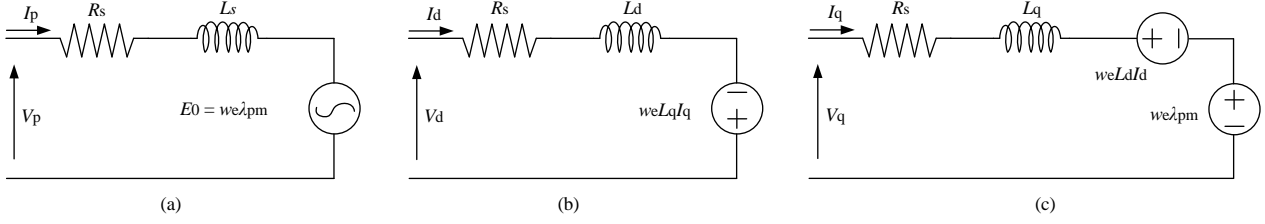
Fig. 18: ECMs of a PMSM: (a) single phase ECM, (b) d-axis ECM, (c) q-axis ECM.

Laboratory Test Setup and Control Architecture of the PMSM

To control the drive cycle's input speed and torque, a cascaded control technique is employed. Figure 19 illustrates the overall control scheme of the PMSM test bench in the laboratory. The DUT, which is the PMSM presented here, is torque-controlled, and the load machine, which is also a PMSM, is speed-controlled. The choice to torque-control the DUT was based on the goal of obtaining fewer harmonics in the input currents at the machine terminal. Both machines side inverters operate at a switching frequency of 20 kHz. A maximum torque per ampere (MTPA) control scheme is used for the current controllers.
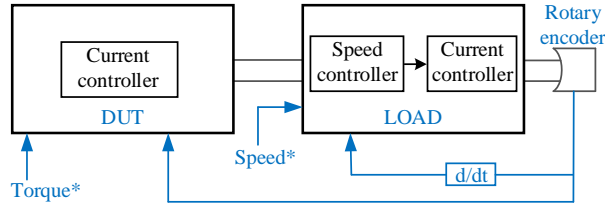
Fig. 19: Drive cycle control scheme of the PMSM in the laboratory test bench, * denotes that the value is commanded.

References

Ahn, S., Song, W. and Min, S. (2023), 'Multiobjective Optimization of a Traction Motor in Driving Cycles Using a Coupled Electromagnetic–Thermal 1D Simulation', *International Journal of Energy Research* **2023**, e8854778.

Ba, X., Gong, Z., Guo, Y., Zhang, C. and Zhu, J. (2022), 'Development of Equivalent Circuit Models of Permanent Magnet Synchronous Motors Considering Core Loss', *Energies* **15**(6), 1995.

Barcaro, M. and Bianchi, N. (2013), 'Design considerations of permanent magnet machines for automotive applications', *COMPEL - The international journal for computation and mathematics in electrical and electronic engineering* **32**(1), 248–277.

Bergfried, C., Späck-Leigsnering, Y., Seebacher, R., Eickhoff, H. and Muetze, A. (2023), 'Thermal Finite Element Modeling and Simulation of a Squirrel-Cage Induction Machine'. available at: https://arxiv.org/abs/2311.08821.

Deutsche Forschungsgemeinschaft DFG (2022), 'TRR 361: Computational Electrical Machine Laboratory: Thermal Modeling, Transient Analysis, Geometry Description and Robust Design'. available at: https://gepris.dfg.de/gepris/projekt/492661287?context=projekt&task=showDetail&id=492661287& (accessed 16 May 2024).

Dhakal, P. K. (2024), 'CREATOR Case: Permanent Magnet Synchronous Motor Data'. Graz University of Technology. available at: https://doi.org/10.3217/sns1d-77m43.

Dhakal, P. K., Heidarikani, K. and Muetze, A. (2023), Down-scaling of drive cycles for experimental drive cycle analyses, *in* '12th International Conference on Power Electronics, Machines and Drives (PEMD 2023)', Vol. 2023, Brussels, Belgium, pp. 271–276.

DieselNet (2011), 'Emission Test Cycles'. available at: https://dieselnet.com/standards/cycles/index.php (accessed 23 September 2024).

Eickhoff, H. T., Seebacher, R. and Muetze, A. (2021), 'Space Harmonics and Saturation Interaction in Fault-Tolerant Induction Machine Drives Due to a Zero-Sequence Stator Current', *IEEE Transactions on Industry Applications* **57**(5).

Fedesoriano (2021), 'Synchronous Machine Dataset'. availalbe at: https://www.kaggle.com/datasets/fedesoriano/synchronous-machine-dataset (accessed 23 September 2024).

Ferretti, J. (2022), 'SPM demagnetization dataset'. availalbe at: https://www.kaggle.com/datasets/mrjacopong/spm-demagnetization-dataset (accessed 23 September 2024).

Gallileo Ferraris Contest (2024). available at: https://cadema-polito.github.io/GalFer_contest/ (accessed 26 September 2024).

Gobbi, M., Sattar, A., Palazzetti, R. and Mastinu, G. (2024), 'Traction motors for electric vehicles: Maximization of mechanical efficiency – A review', *Applied Energy* **357**, 122496.

Guzzella, L. and Amstutz, A. (2005), *The QSS toolbox manual*.

Heidarikani, K. (2024), 'CREATOR Case: Induction Motor Data'. Graz University of Technology. available at: https://doi.org/10.3217/kh3v7-dhn98.

Hendershot, J. R. and Miller, T. J. E. (2010), *Design of Brushless Permanent-magnet Machines*, Motor Design Books.

Hwang, S.-W., Ryu, J.-Y., Chin, J.-W., Park, S.-H., Kim, D.-K. and Lim, M.-S. (2021), 'Coupled Electromagnetic-Thermal Analysis for Predicting Traction Motor Characteristics According to Electric Vehicle Driving Cycle', *IEEE Trans. Veh. Technol.* **70**(5), 4262–4272.

JSOL Corporation (1983), 'Simulation Technology for Electromechanical Design : JMAG'. available at: https://www.jmag-international.com/products/ (accessed 9 September 2024).

JSOL Corporation (2022), '[JAC017] Inductance Analysis of an IPM Motor | Simulation Technology for Electromechanical Design : JMAG'. available at: https://www.jmag-international.com/catalog/17_ipmmotor_inductance/download/ (accessed 9 September 2024).

Kojooyan-Jafari, H., Monjo, L., Córcoles, F. and Pedra, J. (2015), 'Using the instantaneous power of a free acceleration test for squirrel-cage motor parameters estimation', *IEEE Transactions on Energy Conversion* **30**(3), 974–982.

Krause, P., Wasynczuk, O., Sudhoff, S. D. and Pekarek, S. (2013), *Introduction to the Design of Electric Machinery*, Wiley-IEEE Press, pp. 583–622.

LCR meter (2023). available at: https://en.wikipedia.org/w/index.php?title=LCR_meter&oldid=1166233223 (accessed 10 September 2024).

Li, M., Mohammadi, M. H., Rahman, T. and Lowther, D. (2017), 'Analysis and design of electrical machines with material uncertainties in iron and permanent magnet', *COMPEL - The international journal for computation and mathematics in electrical and electronic engineering* **36**(5), 1326–1337.

Mese, E., Ayaz, M. and Tezcan, M. M. (2016), 'Design considerations of a multitasked electric machine for automotive applications', *Electric Power Systems Research* **131**, 147–158.

Oberkampf, W. L. and Roy, C. J. (2010), *Verification and Validation in Scientific Computing*, Cambridge University Press, Cambridge.

Pyrhonen, J., Jokinen, T. and Hrabovcova, V. (2009), *Design of Rotating Electrical Machines*, John Wiley & Sons.

Rimpas, D., Kaminaris, S. D., Piromalis, D. D., Vokas, G., Arvanitis, K. G. and Karavas, C.-S. (2023), 'Comparative Review of Motor Technologies for Electric Vehicles Powered by a Hybrid Energy Storage System Based on Multi-Criteria Analysis', *Energies* **16**(6), 2555.

Shimizu, Y. (2023), 'Dataset for Iron Losses of IPMSMs'. available at: https://www.kaggle.com/datasets/uuuuuuuuu/dataset-iron-losses-ipmsms (accessed 23 September 2024).

TEAM Problems – International Compumag Society (2018). available at: https://www.compumag.org/wp/team/ (accessed 26 September 2024).

Tessarolo, A., Mohamadian, S. and Bortolozzi, M. (2015), 'A new method for determining the leakage inductances of a nine-phase synchronous machine from no-load and short-circuit tests', *IEEE Transactions on Energy Conversion* **30**(4), 1515–1527.

Weinper, K. and Tomczak, L. (2021), 'HOW TO BE FAIR? OPEN PUBLICATIONS AND RESEARCH DATA AT THE LUBLIN UNIVERSITY OF TECHNOLOGY', *TASK Quarterly* **25**(4), 491–498. available at: https://doi.org/10.34808/tq2021/25.4/r (accessed: 24 October 2024).

Wilkinson, M. D., Dumontier, M. and et al. (2016), 'The FAIR Guiding Principles for scientific data management and stewardship', *Scientific Data* **3**(1), 160018. available at: https://doi.org/10.1038/sdata.2016.18 (accessed 24 October 2024).

Österreichischer Wissenschaftsfonds FWF (2022), 'F90 - Computer-aided electrical machine laboratory'. available at: https://www.fwf.ac.at/entdecken/im-fokus/spezialforschungsbereiche (accessed 16 May 2024).